INTERNATIONAL JOURNAL OF HYDROGEN ENERGY XXX (2017) 1–10

Available online at www.sciencedirect.com

ScienceDirect

journal homepage: www.elsevier.com/locate/he

Hydrogen production by crude glycerol steam reforming over Ni–La–Ti mixed oxide catalysts

Santiago Veiga [a,*], *Ricardo Faccio* [b], *Darío Segobia* [c], *Carlos Apesteguía* [c], *Juan Bussi* [a]

[a] *Lafidesu, DETEMA, Facultad de Química, Universidad de la República, General Flores 2124, Montevideo, 11800, Uruguay*

[b] *Centro NanoMat/CryssMat-Lab, DETEMA, Facultad de Química, Universidad de la República, General Flores 2124, Montevideo, 11800, Uruguay*

[c] *Catalysis Science and Engineering Research Group (GICIC), INCAPE, UNL-CONICET, Predio CCT Conicet, Paraje El Pozo, Santa Fe, 3000, Argentina*

ARTICLE INFO

Article history:
Received 16 August 2017
Received in revised form
17 October 2017
Accepted 19 October 2017
Available online xxx

Keywords:
Crude glycerol
Hydrogen
Ni–La–Ti mixed oxides
Steam reforming

ABSTRACT

The production of H_2-rich gaseous mixtures from steam reforming of crude glycerol was investigated on ternary Ni–La–Ti catalysts. Ni–La–Ti mixed oxides containing 15 wt% of Ni and a La/Ti atomic ratio of 1 were prepared by a coprecipitation method and characterized by a variety of physical and spectroscopic techniques. Samples were calcined in air at 700 °C or 850 °C for 2 h. Ni–La–Ti samples calcined at 700 °C (NiLaTi700) showed a well-defined NiO phase and an amorphous La–Ti mixed oxide, while those calcined at 850 °C (NiLaTi850), exhibited two well defined phases of NiO and $LaTiO_3$ perovskite, respectively. NiO was completely reduced to metallic Ni on both solids under pure H_2 at 650 °C and the resulting Ni^0 phase remained as a separate phase under the steam reforming conditions. Standard catalytic tests for the steam reforming of glycerol were performed at 500 °C or 650 °C by feeding the fixed-bed tubular reactor with a crude glycerol:water solution containing 30 wt% glycerol. The best results were achieved on NiLaTi700 at 650 °C, obtaining H_2 yields and H_2/CO_2 molar ratios close to the theoretical values predicted by the steam reforming reaction stoichiometry. A slight activity decay was observed on NiLaTi700 with the progress of the reaction, probably reflecting the formation of small amounts of coke.

Introduction

Glycerol is the main by-product of the vegetable oils transesterification with methanol which is nowadays the most widespread method for biodiesel production. At industrial level, crude glycerol (CG) is a low-value product that is obtained in a glycerol:biodiesel = 1:10 per weight ratio and contains impurities such as methanol, solvents and inorganic salts [1]. Because of the increasing worldwide biodiesel production, the development of efficient technologies to convert crude glycerol into more valuable products has been widely investigated in order to offset the cost in biodiesel production [2,3]. In particular, steam reforming is an attractive method to process glycerol because hydrogen-rich gas mixtures that can

* *Corresponding author.*
E-mail addresses: sveiga@fq.edu.uy, sanveiga@gmail.com (S. Veiga).

https://doi.org/10.1016/j.ijhydene.2017.10.118

be used to generate electricity directly in either a fuel cell or a gas turbine are obtained [4,5]. Several research groups have paid attention to the catalytic steam reforming (SR) of pure glycerol [6–11]. The gas-phase reaction takes place according to the following stoichiometry [8,10]:

$$C_3H_8O_3 + 3\,H_2O \leftrightarrow 3\,CO_2 + 7\,H_2 \quad (1)$$

In contrast, very few studies have been performed using CG as carbon source [11–13], probably because the catalyst is often rapidly deactivated by the CG impurities. Table 1 summarizes the results reported in the literature.

Some of the impurities, such as methanol, are easily decomposed, so its removal step, which is required to upgrade crude glycerol to value-added products, is avoided by using the steam reforming process. Other impurities, such as unreacted triglycerides and biodiesel catalyst residues, are undesirable to the reforming process since they contribute to increase deposit formation, pore clogging and catalyst deactivation. Catalytic bed regeneration becomes thus a key aspect to be handled in this case in order to extent catalyst lifetime and reduce energy consumption as much as possible. Nickel catalysts are particularly attractive for promoting the CG steam reforming because of the high activity of Ni and its lower cost compared with noble metals (Ru, Rh, Pt) [8,15,16]. Different oxides like SiO_2, Al_2O_3, MgO, La_2O_3, CeO_2, ZrO_2, TiO_2 or their mixtures are used to provide high Ni dispersion as well as suitable thermal, mechanical and chemical properties [17,18]. Several deactivation phenomena may take place in steam reforming reactions. On one hand, carbon deposits are formed by side reactions involving the formation of non-volatile compounds by polymerization of CHx species and/or CO dissociation. The tendency to carbon deposition depends on the atomic ratio O/C and H/C in the feed gas. Lower H_2O/HC and H_2/CO ratios correspond to higher tendency toward coke formation. On the other hand, metal sintering, and consequently the loss of active sites, is favored under steam reforming conditions [17,19–21]. The support properties play a significant role regarding catalyst deactivation; for example, in the case of Ni-based catalysts the following decreasing stability order was observed for glycerol stem reforming: Ni/SiO_2 > Ni/ZrO_2 > Ni/Al_2O_3 [17]. Catalyst stability and activity also depends on the preparation method. It has been reported that Ni catalysts prepared by solid phase extraction (SFE) techniques display well stabilized Ni species and are very active and selective in steam reforming reactions [22–25]. Ni crystallites highly dispersed into a suitable oxide support are obtained after a thermal and/or reducing treatment of a mixed oxide precursor. In previous works [26–28] we have studied the steam reforming of ethanol and glycerol on ternary Ni–La–Zr mixed oxides containing 5 wt% and 10 wt% of Ni. Nanosized crystallites of metallic Ni and a pyrochlore compound $La_2Zr_2O_7$ remained as the unique phases under typical reforming conditions. High conversion to gas phase products and H_2 yields close to the thermodynamic limits were achieved. Good stability was also observed and ascribed to very low carbon formation. Other metals commonly used in the preparation of conventional supported catalysts can be used for the preparation of Ni catalysts with the same techniques. In this sense, the ternary Ni–La–Ti system was selected as a starting material on the basis of its properties to yield metallic Ni and a lanthanum titanate compound under typical reforming experimental conditions [29]. Additionally, lanthanum titanates are known by their high thermal stability and chemical resistance against typical corrosion agents including alkaline metal compounds [30]. Chemical inertness could contribute to preserve not only textural and structural properties of the catalyst but also the properties (amount and intrinsic activity) of the different active sites involved in the whole reaction mechanism.

The aim of the present work is to study the ternary Ni–La–Ti mixed oxide system for the preparation of Ni catalysts by a SFC method and their behavior in the steam reforming of glycerol. Crude glycerol without any process of purification was used in the reforming tests.

Materials and methods

Materials

Nickel nitrate $Ni(NO_3)_2{\cdot}6H_2O$, lanthanum nitrate $La(NO_3)_3{\cdot}6H_2O$, titanium isopropoxide ($Ti(OCH(CH_3)_2)_4$) and oxalic acid (HO_2CCO_2H) were purchased from Sigma–Aldrich. Ethanol was purchased from Carlo Erba. All chemicals were reagent-grade and were used as received. The CG used in the present work mainly consists of 64 wt% glycerol, inorganic salts 5.7 wt%, methanol and water lower than 5 wt% and polyglycerol impurities up to 26 wt%, provided by the manufacturer. Potassium methylate was used as transesterification catalyst. CG composition was determined by elemental analysis (Thermo Scientific Flash 2000). Other CG characterizations were reported elsewhere [14]. The calculated average elemental molar formula for CG determined from these results was $C_{3.5}H_{9.0}O_{3.1}$ and was used to calculate conversion and yield parameters.

Table 1 – Studies of CG steam reforming.

Method	Catalyst	Reaction conditions			Stability	Reference
		S/C	T (°C)	$WHSV_{GC}$[b] (h^{-1})		
SR	Pt (0, 5%)/Al_2O_3	1.35	800	0.79–1.58	10 h	[11]
SESR[a]	20%Ni–20%Co/HT	3.0	525–600	0.9	150 min	[12]
SESR	18%NiO/Al_2O_3	3.0	400–700	0.34	15 min	[13]
SR	Ni10%Mg10%/AC	3.7	650	3	6 h	[14]

[a] Sorption enhanced steam reforming.
[b] $WHSV_{GC}$ defined as the ratio between the mass flow rate of crude glycerol fed and the mass of catalyst.

Please cite this article in press as: Veiga S, et al., Hydrogen production by crude glycerol steam reforming over Ni–La–Ti mixed oxide catalysts, International Journal of Hydrogen Energy (2017), https://doi.org/10.1016/j.ijhydene.2017.10.118

Catalyst preparation

The catalysts were synthesized by a coprecipitation method. A certain amount of nickel and lanthanum nitrates and titanium isopropoxide were dissolved in absolute ethanol. Then, oxalic acid was added to the solution. The resulting precipitates were aged for 1 h at 80 °C. After that, the suspension was filtered and washed with absolute ethanol. The obtained solid was dried overnight at 100 °C and then calcined in two stages: first at 550 °C for 24 h and finally at 700 or 850 °C for 2 h. The resulting catalysts contained 15 wt% of Ni on a weight basis and a La/Ti atomic ratio of 1. Catalysts will be denoted as NiLaTiX, where X is the final calcination temperature.

Catalyst characterization

BET surface area, pore volume and pore size were measured by N_2 physisorption at −196 °C in a Beckman-Coulter SA 3100 sorptometer. Before measurement the samples were outgassed at 200 °C for 10 h in order to desorb moisture and other weakly adsorbed residues.

Crystal structures of fresh, reduced and used catalysts were determined by XRD analysis, using a Rigaku Ultima IV diffractometer with CuKα radiation. Diffractograms were recorded in the 2θ range between 10° and 60° with a step of 0.02° and an integration time of 3 s per step. Phases present in the samples were identified by comparison with ICDD files.

The morphological SEM analysis and EDS microanalysis of the tested catalysts were studied using scanning electron microscopy (Jeol JSM-5900V). Before and after use in reforming tests, catalysts were subject to thermogravimetric analysis (TGA) (Shimadzu TGA-50) under 50 mL min^{-1} air flow, with temperature increasing from 20 °C to 900 °C at a rate of 5 °C min^{-1}.

Reduction of the catalyst was studied by temperature programmed reduction (TPR) using 5% H_2/Ar gaseous mixture at 60 cm^3 min^{-1} STP. The sample size was 150 mg. Samples were heated from 25 to 850 °C at 10 °C min^{-1}. Hydrogen consumption was measured by mass spectrometry (MS) in a Baltzers Omnistar unit.

Raman was used to characterize the nature of carbon formed after reaction. Confocal Raman spectroscopy was performed using WITec Alpha 300-R confocal Raman spectrometer with a 532 nm laser wavelength. The laser power used was 30 mW and confocal Raman spectra were collected by averaging a set of 4 spectra of 0.05 s integration time in different areas to assess the homogeneity of the investigated material.

Carbon build-up on the spent catalysts was analyzed for its C and H contents (Thermo Scientific Flash 2000).

Catalytic tests

Crude glycerol steam reforming (CGSR) tests were carried out in a 1.2 cm diameter and 30 cm length stainless steel tubular fixed bed reactor located inside a tubular electric furnace.

The catalyst bed configuration consists in a 2 g SiC bed placed above 0.2 g of the catalyst. Before reaction, the catalyst was reduced under a 30 mL min^{-1} pure hydrogen flow by heating from room temperature to 650 °C, at a rate of 10 °C min^{-1} and keeping the final temperature for 1 h. Following reduction, the H_2 flow was stopped and the reactor purged with argon. Then the reactor was brought to the reaction temperature under argon. After that, the water:CG solution (30 wt% of CG) was fed at 2.0 mL h^{-1} with a peristaltic pump (Cole Parmer 74900 Series) through a device consisting of two concentric tubes which are placed into the tubular reactor. Water:CG solution was injected into the internal tube (0.2 mm i.d.) and argon through the external one (2.1 mm i.d.). With this device, partial vaporization of glycerol and other compounds in the CG would occur in the sprayed liquid solution along with water. Proper adjustment of the distance of the device to the catalytic bed allowed to obtain a stable feed of the solution. The experiments were performed at atmospheric pressure with time-on-stream (TOS) of 10 h and reaction temperatures of 500 and 650 °C. The steam-to-carbon (S/C) molar ratio was equal to 3.7. Under these conditions the gas hourly space velocity (GHSV) was 20 L $h^{-1}g^{-1}$ and $WHSV_{GC}$ defined as the ratio between the mass flow rate of crude glycerol fed and the mass of catalyst was 3 h^{-1}. Unreacted glycerol and some of the condensable reaction products were retained in a dry ice trap at the reactor exit. A 45 h stability test was performed with the NiLaTi700 catalyst under GHSV = 40 L $h^{-1}g^{-1}$ and $WHSV_{GC}$ = 6 h^{-1} conditions. After 15 h of operation regeneration steps were carried out at 650 °C for 1 h under O_2 atmosphere (20 mL min^{-1}).

Non-condensable products, mainly H_2, CO, CO_2, CH_4, C_2 (ethane and ethylene) and C_3 (propane and propylene) hydrocarbons, were analyzed with a gas-chromatograph (Shimadzu GC-14B) equipped with FID and TCD detectors in series and columns Supelco CarboxenTM-1000 and Porapak Q. At the end of reaction, glycerol and condensed liquid products were collected and analyzed by HPLC (Shimadzu Prominence) equipped with a Rezex RHM-Monosaccharide H+ (8%) column and a refractive index detector.

Catalytic performance was evaluated in terms of glycerol conversion, carbon conversion to non-condensable products ($X_{C,GAS}$) and hydrogen yield which were determined as:

$$X_{Gly}(\%) = 100 * \frac{Gly_{in} - Gly_{out}}{Gly_{in}} \quad (2)$$

$$X_{C,GAS}(\%) = 100 * \frac{\sum F_{C,i} * n_i}{F_{C,IN}} \quad (3)$$

$$X_{C,LIQ}(\%) = 100 * \frac{C_{liq.\ products}\ (g)}{C_{FED}\ (g)} \quad (4)$$

$$H_2\ Yield\ (\%) = 100 * \left(\frac{F_{H_2}}{8.4 * F_{CG}}\right) \quad (5)$$

where $F_{C,i}$ is the molar flow of product i (i = CO, CO_2, CH_4, C_2, C_3); n_i the number of carbon atoms in product i; $F_{C,IN}$ is the molar flow of carbon atoms in the CG-water solution fed to the reactor and calculated over the 94.3% of the total weighted amount of CG used for its preparation (5.7% corresponds to the ash fraction determined by calcination); $C_{liq,\ products}$ is the total mass of carbon in products retained in the liquid aqueous solution in the dry ice trap (excluding glycerol); C_{FED} is the

Please cite this article in press as: Veiga S, et al., Hydrogen production by crude glycerol steam reforming over Ni–La–Ti mixed oxide catalysts, International Journal of Hydrogen Energy (2017), https://doi.org/10.1016/j.ijhydene.2017.10.118

total mass of carbon in the CG-water solution fed during the test; F_{H2} is the molar flow rate of H_2 (mol min^{-1}); F_{CG} is the molar flow rate of CG (mol min^{-1}) and 8.4 is the theoretical maximum of H_2 per mol of CG according to Equation (6) derived from the elemental analysis results of CG composition:

$$C_{3.5}H_{9.0}O_{3.1} + 3.9H_2O \leftrightarrow 3.5CO_2 + 8.4H_2 \quad (6)$$

Results and discussion

Catalyst characterization

Fig. 1 shows the thermograms along with derivatives of CG and the solid residue found in the catalytic bed in experiments at 500 °C. CG shows the main mass loss between 120 °C and 270 °C corresponding to glycerol decomposition. A second weight loss takes place between 420 °C and 490 °C and corresponds to the thermal degradation of impurities such as the fatty acid methyl esters and that of their residues from early degradation of glycerol [31].

For the solid residue remaining over the catalytic bed after the steam reforming test, the TG shows a weight loss at the same high temperature range thus revealing that it corresponds to the combustion of the fatty fraction which is not reformed under these experimental conditions. The inset to the Figure shows the image of the brownish residues remaining above the SiC bed at the end of the test. Weight losses above 490 °C are more clearly observed in this analysis and it may correspond to the thermal decomposition of potassium carbonate [32]. Fig. 2 shows the weight loss and derivative weight profile of the Ni–La–Ti precursors: i) dried at 100 °C (NiLaTi100) and ii) calcined at 550 °C for 24 h (NiLaTi550). For the NiLaTi100, mass loss below 200 °C was most likely due to the removal of physisorbed and bulk ethanol that were initially present in the sample. Starting at 270 °C, a rapid weight loss process was initiated, attributed to the decomposition of metal oxalates. This process was continued at elevated temperatures in the order of 800 °C. For

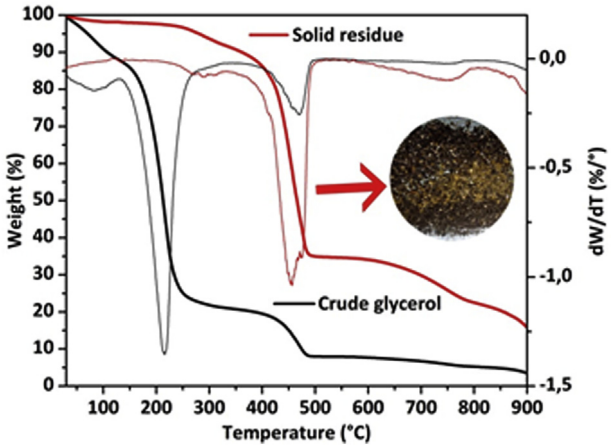

Fig. 1 – Weight loss and derivative weight profiles of CG and the solid residue obtained after a 500 °C reforming test.

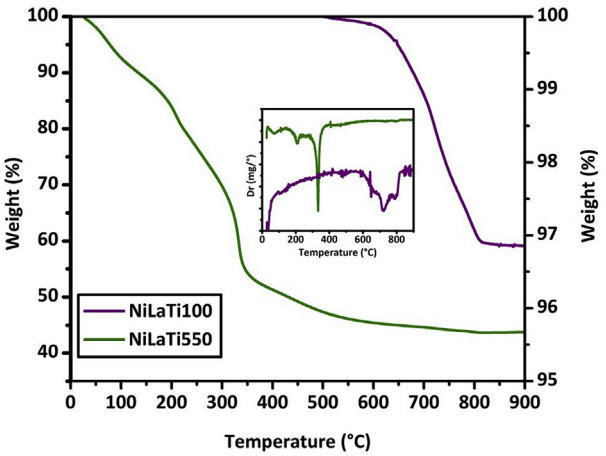

Fig. 2 – Weight loss and derivative weight profiles for temperature-programmed calcination of NiLaTi precursor and NiLaTi550.

NiLaTi550, the mass loss starts close to 550 °C and is probably due to the combustion of carbon residues formed during metal oxalate decomposition.

X-ray powder diffraction patterns for calcined catalysts (Fig. 3) showed the presence of two peaks at 2θ = 37.4 and 43.4

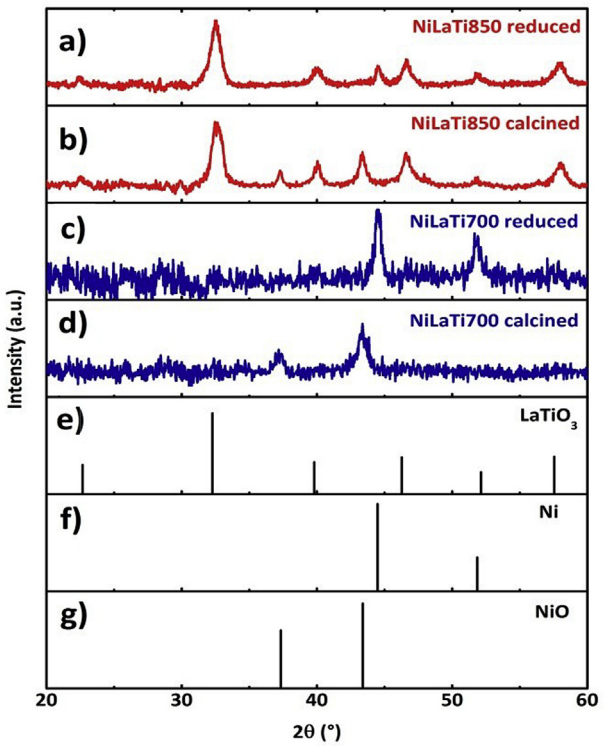

Fig. 3 – XRD patterns of NiLaTi catalysts: (a) reduced NiLaTi850, (b) fresh NiLaTi850, (c) reduced NiLaTi700, (d) fresh NiLaTi700 and (e–g) standard XRD cards of $LaTiO_3$, Ni and NiO respectively.

Please cite this article in press as: Veiga S, et al., Hydrogen production by crude glycerol steam reforming over Ni–La–Ti mixed oxide catalysts, International Journal of Hydrogen Energy (2017), https://doi.org/10.1016/j.ijhydene.2017.10.118

ascribed to nickel oxide phase. These can be assigned to (111) and (200) of the lattice plane of the cubic NiO. No peaks related with La and Ti were observed in NiLaTi700, thus suggesting that these metals are present as amorphous oxides homogeneously distributed in the solid structure. NiLaTi850 showed six additional peaks located at $2\theta = 22.7$, 32.3, 39.8, 46.3, 52.1 and 57.6 ascribed to $LaTiO_3$ perovskite in a cubic structure with *Pm*-3m space group. Reflections corresponding to metallic nickel at $2\theta = 44.5$ and 51.9 appear in both catalysts after reduction in pure hydrogen at 650 °C for 1 h revealing that NiO was totally reduced. $LaTiO_3$ reflections remain unchanged thus showing its stability under these reducing treatment.

The N_2 adsorption–desorption isotherms for the freshly calcined catalysts are depicted in Fig. 4. Pore volume distribution profiles are also included. All isotherms resembled the Type IV isotherm based on IUPAC classification, with A-type hysteresis loops indicating the presence of non-porous particles and interparticle porosity due to pore space located between grains.

Table 2 shows the textural parameters for the fresh catalysts. Low BET areas are similar to those already reported in previous works for others coprecipitated catalysts prepared by the same technique [26–28]. The decrease in BET area for the catalyst calcined at high temperature may be attributed to sintering taking place under more severe thermal treatment conditions. EDS elemental analysis showed that surface nickel compositions and Ni/(La + Ti) ratios agree well with the theoretical value (15 wt% and 0.35 respectively). The crystallite size of NiO particle estimated from Scherrer equation [33] on the fresh catalysts was about 14.5 and 19.6 nm for NiLaTi700 and NiLaTi850, correspondingly.

H_2-TPR measurements were carried out in order to investigate the reducibility of calcined catalysts. Fig. 5 shows the H_2 consumption profiles and their deconvolution into Gaussian peaks. A good fit between the computed peaks (black line) and experimental curve (bold line) could be observed. The

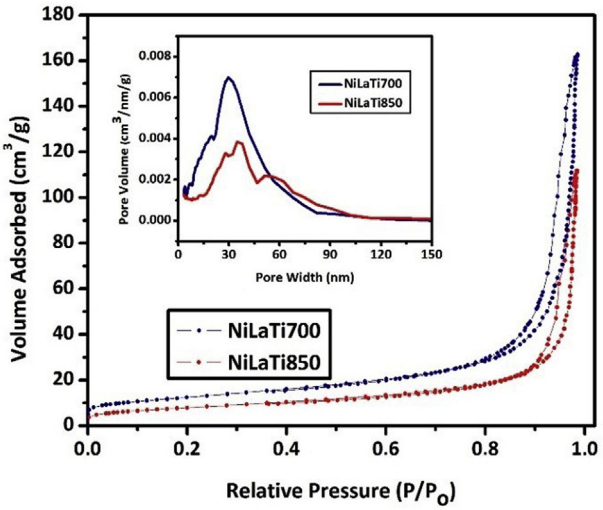

Fig. 4 – N_2 adsorption–desorption isotherms, and BJH pore size distribution for NiLaTi catalysts.

Table 2 – Structural characteristics of fresh Ni–La–Ti catalysts.

Parameter	NiLaTi700	NiLaTi850
BET ($m^2\ g^{-1}$)	44	29
Pore volume ($cm^3\ g^{-1}$)	0.27	0.19
Pore diameter (nm)	25	26
Ni (wt%)[a]	14.4	14.2
Ni/(La + Ti) ratio[a]	0.34	0.34
d_{NiO} (nm)[b]	14.5	19.6

[a] Determined from EDS chemical analysis.
[b] Calculated from the (200) reflection of NiO in XRD.

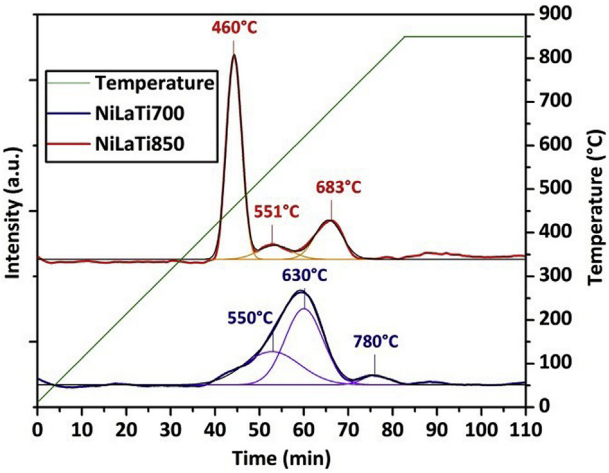

Fig. 5 – Deconvolution of the TPR profile for Ni–La–Ti catalysts.

NiLaTi700 profile shows the reduction peak at the lowest temperature formed by the sum of two peaks (with reduction temperatures at 550 and 630 °C) and can be associated to NiO outside and within the amorphous oxide structure. The peak at 780 °C can be related to H_2 reacting with the O_2 released along with the formation of the perovskite phase with an oxygen-deficient crystalline network [34]. For NiLaTi850 catalyst a peak centered at 460 °C suggest a greater exposure of Ni species in the biphasic system and/or a lower energy to be reduced. This can be favored by the formation of the $LaTiO_3$ perovskite, as shown in XRD results, which should be accompanied by stronger interactions between La and Ti metals within that structure and a weakening of their interactions with the NiO phase. Recent results of our group with a Ni–La–Sn mixed oxide clearly reveals this effect for the biphasic system NiO-$La_2Sn_2O_7$ which is formed [35]. Another two peaks at 551 °C and 683 °C may be attributed to small particles of NiO incorporated in the perovskite support having strong particle–support interactions.

Table 3 summarizes the results obtained in the H_2-TPR measurements. It is shown that Ni reducibility (determined by the H_2 amount consumed by TPR/theoretical amount of H_2 consumption for total reduction, assuming that NiO is stoichiometrically reduced to Ni^0) is close to unity in both

Please cite this article in press as: Veiga S, et al., Hydrogen production by crude glycerol steam reforming over Ni–La–Ti mixed oxide catalysts, International Journal of Hydrogen Energy (2017), https://doi.org/10.1016/j.ijhydene.2017.10.118

Table 3 – Reducibility and deconvoluted peaks for NiLaTi catalysts.

Catalyst	Reducibility	Deconvoluted peaks					
		1		2		3	
		T_{max} (°C)	H_2 uptake (%)	T_{max} (°C)	H_2 uptake (%)	T_{max} (°C)	H_2 uptake (%)
NiLaTi700	0.987	550	37.5	630	57.5	780	5.0
NiLaTi850	0.969	460	66.9	551	10.0	683	23.1

catalysts. It can be also observed that NiLaTi850 contains a larger fraction of Ni being reduced at low temperature.

CGSR tests

Table 4 shows results of CGSR tests with both catalysts. Glycerol conversion, calculated from HPLC analysis of the liquid product sample, is almost complete at both temperatures for the 10 h of operation. Total carbon conversion to gas phase products (X_{gas}) over SiC was 32.3% at 650 °C thus showing that it has a limited catalytic activity. At 500 °C, the reactor was plugged after 2 h of operation by formation of solid compounds in the catalytic bed. At this temperature, the capacity of SiC to break C–C bonds is even lower, allowing the glycerol to react by dehydrogenation, dehydration, rearrangement and condensation reactions [36]. These reactions of glycerol and also those of triglycerides impurities can give yield to low volatile polymeric compounds which remain into the reactor. X_{gas} over both catalysts at 500 °C were 36.5 and 34.3% thus revealing a low decomposition of the different reaction intermediates through reactions with rupture of C–C bonds. X_{gas} increased significantly at 650 °C and the highest value was observed on NiLaTi700 (92.0%). This suggests that, in addition to the most reactive components (methanol and glycerol), fatty acids could also react under these reaction conditions leading to gaseous products typical of the reforming reactions [37]. NiLaTi700 also showed the lower amount of carbon deposits thus evidencing that this catalyst is also the most active to promote typical carbon gasification reactions involving H_2O, CO_2 and lattice oxygen. The better performance of the NiLaTi700 catalyst can be explained mainly by the higher surface area of this catalyst and the smallest Ni particle size. The rate of the different reaction paths of the reforming mechanism could thus be improved by the higher amount of active sites involving either Ni and the mixed oxide compound. A higher carbon gasification rate could also be expected in this catalyst and thereby smaller amounts of carbon deposits as shown in Table 3. Changes in the nature of active sites could also affect the catalytic activity. On one hand, stronger interactions between Ni and the other two metal oxides are expected to occur in NiLaTi700 and can also contribute to the improvement of the catalytic performance. In this sense, the literature reports the beneficial effect of La_2O_3 to facilitate Ni dispersion and to increase the basic sites population of the support [38–41]. Stronger interactions between the active phase and the support are also reported in a TiO_2-supported Ni catalyst with a proper thermal activation, preserving the catalyst from sintering and improving its stability in reforming reactions [42]. On the other hand, the NiLaTi850 contains the $LaTiO_3$ perovskite with oxygen vacancies which can increase the mobility of lattice oxygen and their interactions with carbon formed mainly over Ni sites [43].

Table 5 shows product selectivity for the gaseous mixtures obtained in the reforming tests. At 650 °C H_2 yields as well as H_2/CO_2 molar ratios approximate the theoretical ones according to the stoichiometry shown in Equation (6) (70,6% and 2.4 respectively). The better reforming performance of the NiLaTi700 catalyst is evidenced mainly by the lower CH_4 selectivity and by the absence of other light hydrocarbons (C_2 and C_3).

Negligible amounts of intermediate liquid products were detected for both catalysts at the two temperatures tested. These liquid products were mainly ethanol, methanol, acetaldehyde, acetone, acetic acid, ethane-1,2-diol, propane-1,2-diol in agreement with those reported in the literature for both steam and aqueous phase glycerol reforming [44,45]. At low temperatures, polymeric compounds would be preferably formed starting from these compounds leading to coke formation [36,46–48]. At higher temperatures the basic properties of the catalysts, mainly due to the presence of La, as well as the higher rate of pyrolysis and steam gasification reactions allow an increased reaction rate of all the intermediate compounds giving yield to gaseous products [46,48,49].

The carbon balance for all the runs was estimated with data summarized in Table 4. A large fraction of the total carbon was not recovered at 500 °C. Due to low amount of liquid

Table 4 – Catalytic results in CGSR tests using Ni–La–Ti catalysts (P = 1 bar; GHSV = 20 L $h^{-1}g^{-1}$, $WHSV_{CG}$ = 3 h^{-1}, TOS = 10 h).

Catalyst	Temp. (°C)	X_{gly} (%)	X_{gas} (%)	X_{liq} (%)	C_{dep} ($mg_C/g_{C,in}$)	C balance (%)
NiLaTi700	500	99.5	36.5	0.7	15.7	38.8
	650	99.7	92.0	0.6	39.4	96.5
NiLaTi850	500	99.3	34.3	0.7	18.9	36.9
	650	99.5	74.5	0.8	199	95.2

Table 5 – Gaseous products distribution in CGSR tests using Ni–La–Ti catalysts (P = 1 bar; GHSV = 20 L $h^{-1}g^{-1}$, $WHSV_{CG}$ = 3 h^{-1}, TOS = 10 h).

Catalyst	Temp. (°C)	Gaseous products distribution (mol%)					
		H_2	CO_2	CO	CH_4	C_2	C_3
NiLaTi700	500	57.1	29.8	7.6	3.4	1.3	1.2
	650	66.3	27.7	4.1	1.9	–	–
NiLaTi850	500	55.8	29.6	8.0	3.9	1.5	1.2
	650	66.4	23.6	5.0	2.5	1.8	1.0

Please cite this article in press as: Veiga S, et al., Hydrogen production by crude glycerol steam reforming over Ni–La–Ti mixed oxide catalysts, International Journal of Hydrogen Energy (2017), https://doi.org/10.1016/j.ijhydene.2017.10.118

products (X_{liq} = 0.6–0.8%), the unaccounted carbon is likely due to carbon being retained as solid deposits on the reactor walls and the SiC bed prior to reaching the catalyst. At 650 °C, carbon recovery is almost total and differences can be due to other reaction products which may be present at concentrations below the detection limits of the gas chromatograph.

Fig. 6 shows H_2 evolution as a function of time for all the 10 h tests. H_2 yield was in the range 20–30% for both catalysts at 500 °C and variations do not exceed 5%. At 650 °C, NiLaTi700 allows an initial H_2 yield of 94% which continuously decreases until a final value of 80–82%. NiLaTi850 exhibits a lower initial H_2 yield (69%) together with a progressive decay until ~50% at the end of the test. These results show that both catalysts deactivate but NiLaTi700 does it to a lesser extent. Deactivation in CGSR processes is reported by very few studies. Douette et al. found rapid deactivation with a commercial Ni-based catalyst. The pressure quickly increased and the reactor was found to be filled with sintered deposits [50]. Slin et al. showed H_2 yield decays with an unspecified operating time on a Pt-alumina catalyst working at various temperatures between 580 °C and 780 °C [11].

Differences in the time-dependence of H_2 yields for both catalysts can be related to differences in the amounts of carbon deposits formed by secondary reactions involving polymerization and/or breakage of C–H bonds of intermediate species. The lower decay of H_2 yield observed in NiLaTi700 is thus consistent with the lower amount of residual carbon in this catalyst (Table 3). Physical deposition of the potassium compounds onto the catalyst surface can also result in blockage of sites and/or pores with the subsequent loss of catalytic activity [21].

Post-reaction characterization

The catalysts used in CGSR tests at 650 °C were analyzed after their use in the reforming tests. XRD analysis (Fig. 7) showed that NiLaTi850 has preserved its crystalline structure with regards to the reduced form before the test as shown in Fig. 3.

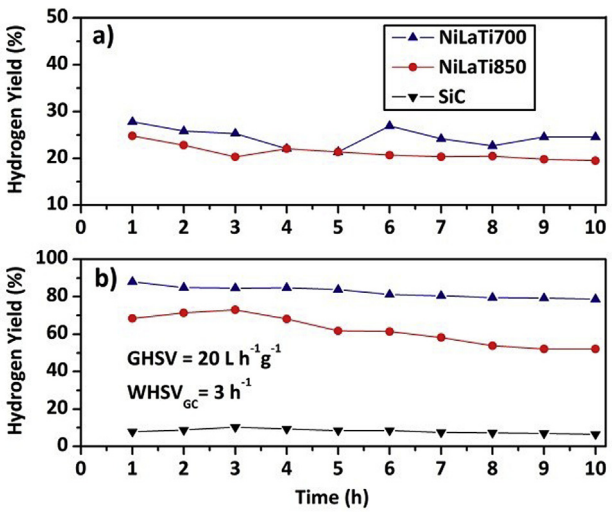

Fig. 6 – Hydrogen yield of NiLaTi catalysts at: (a) 500 °C and (b) 650 °C.

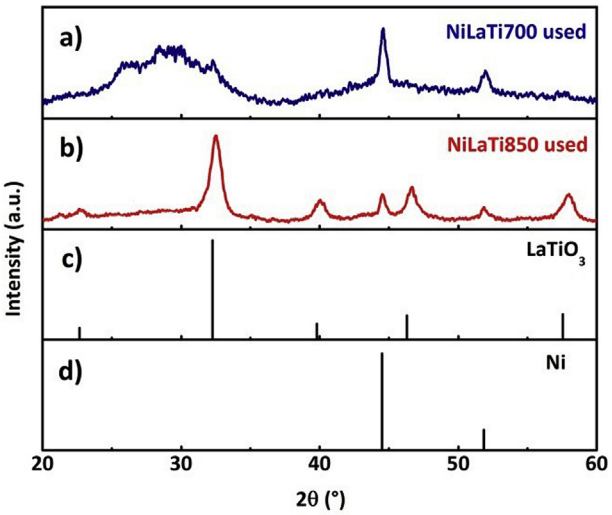

Fig. 7 – XRD patterns of used NiLaTi catalysts: (a) NiLaTi700, (b) NiLaTi850 and standard XRD cards of: (c) $LaTiO_3$ and (d) Ni.

This result confirms the chemical stability of both phases under the CGSR conditions and in the presence of potassium compounds remaining in the reactor. For the catalyst obtained by calcination at 700 °C reflections corresponding to metallic Ni has been preserved, while the wide broad peak located in the range between 2θ = 20°–35° indicates the presence of amorphous phases, that cannot directly be associated to any chemical phase. Nevertheless, the position of this wide peak is consistent with the presence of amorphous carbon [51] or carbonates such as lanthanum oxide carbonate $La_2O_2CO_3$ [52]. $La_2O_2CO_3$ is reported to act as a carbon reservoir to react with deposited carbon around the boundaries of Ni particles, thus avoiding catalyst deactivation [53].

The size of the metallic Ni particles before and after reaction was determined by Scherrer equation using the data from the XRD pattern (111 reflection of Ni). As can be seen in Table 6, smaller Ni particle size was determined for NiLaTi700 catalyst. The degree of sintering was also calculated in CGSR at 650 °C. This result seems to indicate that NiLaTi850 suffered a higher sintering degree. NiLaTi700 catalyst was sintering-resistant under reaction conditions and attributed to the

Table 6 – Metallic Ni particle diameter before and after the steam reforming reaction at 650 °C.

Catalyst	Metallic Ni particle diameter (nm)[a]		Sintering (%)[b]
	Before	After	
NiLaTi700	10.6	11.3	6.6
NiLaTi850	16.7	20.9	25.1

Diameter of the metallic Ni particle before (d_{br}) and after reaction (d_{ar}) determined by XRD.
[a] Calculated from the (1 1 1) reflection of Ni in XRD.
[b] Degree of Ni sintering calculated with the formula: % sintering = 100*(d_{ar} – d_{br})/d_{br}.

Please cite this article in press as: Veiga S, et al., Hydrogen production by crude glycerol steam reforming over Ni–La–Ti mixed oxide catalysts, International Journal of Hydrogen Energy (2017), https://doi.org/10.1016/j.ijhydene.2017.10.118

Table 7 – EDS chemical analysis of NiLaTi catalysts used at 650 °C.

Element (wt. %)	NiLaTi700		NiLaTi7850	
	Before	After	Before	After
Ni	14.4	14.2	14.2	11.6
La	43.4	40.1	44.5	30.3
Ti	19.4	16.7	18.7	14.5
O	22.8	16.4	22.6	21.7
C	–	10.8	–	19.6
K	–	1.8	–	2.3

proper metal–support interaction avoiding particle migration and subsequent coalescence.

EDS results in Table 7 show the amount of carbon and potassium at the surface of used catalysts. NiLaTi850 shows the highest amount of carbon which agrees well with the highest deactivation rate already observed over this catalyst. The amount of potassium that comes from the trans-esterification catalyst was quite similar in both catalysts since the amount fed was the same.

Raman spectra of spent catalysts (Fig. 8) show D and G bands which are commonly used to identify the quality or graphitic nature of carbons [54]. NiLaTi850 showed an average I_{DIG} value (taken from four different Raman spectrum spots) of 0.70, lower than the 1.42 of the NiLaTi700 catalyst. The lower ratio of intensities I_{DIG} for NiLaTi850 points out on higher crystallinity of the carbon formed on this catalyst.

Thermograms for NiLaTi700 and NiLati850 after reaction at 650 °C are shown in Fig. 9. The weight losses are associated to carbon dioxide produced by the complete combustion of carbon-rich deposits in both catalysts and by decomposition of $La_2O_2CO_3$ in NiLaTi700. The larger weight loss in NiLaTi850 is consistent with results obtained by the other characterization techniques used in the present study and confirms the greater tendency of this catalyst to be deactivated by carbon formation.

H_2 production in the CGSR reaction was followed in the 45 h stability test performed with the NiLaTi700 catalyst at 650 °C. As shown in Fig. 10, after the regeneration steps with

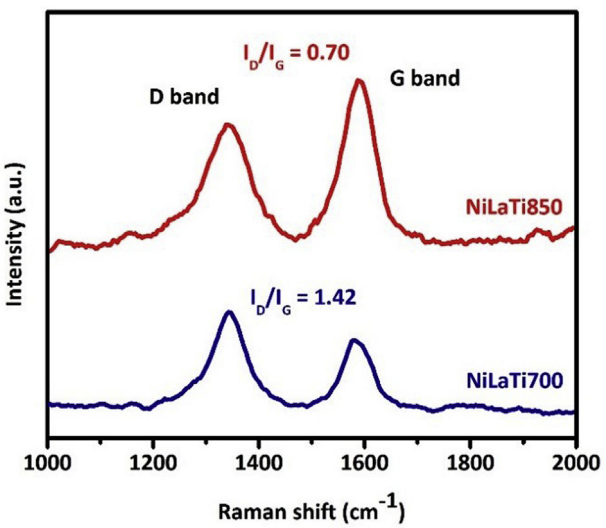

Fig. 8 – Raman spectra of spent catalysts.

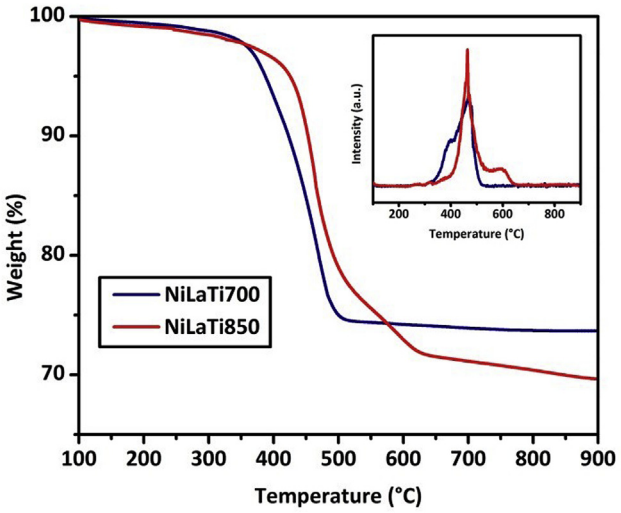

Fig. 9 – TGA and drTGA profiles of NiLaTi catalysts after reaction at 650 °C for 10 h.

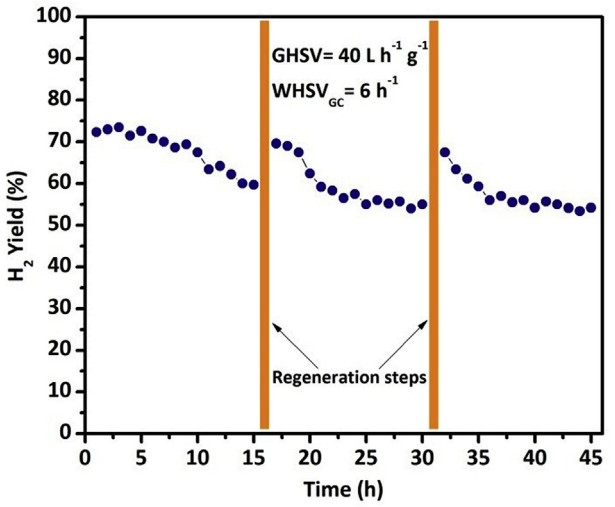

Fig. 10 – Long-term CGSR test with the NiLaTi700 catalyst at 650 °C.

O_2, the production of H_2 returns to values close to those of the beginning, thus confirming that deactivation is mainly due to blockage of sites by carbon deposits. Alkali compounds present in CG can also accumulates inside the reactor and cause clogging in the catalytic bed with the consequent increase of the pressure drop. Nevertheless, alkali deposits may also play a beneficial role since they favor steam gasification reactions due to their active catalytic role [55]. They can also exert a catalytic effect on the gasification of the carbonaceous deposits [56].

Conclusions

Ni–La–Ti mixed oxides prepared by a coprecipitation technique were tested as catalysts in the crude glycerol steam reforming reaction at 500 °C and 650 °C. A calcination temperature of

Please cite this article in press as: Veiga S, et al., Hydrogen production by crude glycerol steam reforming over Ni–La–Ti mixed oxide catalysts, International Journal of Hydrogen Energy (2017), https://doi.org/10.1016/j.ijhydene.2017.10.118

700 °C lead to a solid material containing a well-defined NiO phase and an amorphous mixed oxide containing La and Ti. After calcination at 850 °C, a solid containing two well defined phases, NiO and the $LaTiO_3$ perovskite, is obtained. NiO is easily reduced to metallic Ni on both solids in the presence of pure H_2 at 650 °C and it remains as a separate phase under the steam reforming conditions. The solid obtained at 700 °C displayed the best performance in the steam reforming tests, allowing total glycerol transformation and high selectivity for the production of H_2-rich gaseous mixtures. Low deactivation of this catalyst was observed at 650 °C thus showing highly efficient carbon removal from the boundaries of active sites.

Acknowledgements

National Program for the Development of Basic Sciences (PEDECIBA-PNUD).

REFERENCES

[1] Hu S, Luo X, Wan C, Li Y. Characterization of crude glycerol from biodiesel plants. J Agric Food Chem 2012;60(23):5915–21.
[2] Johnson DT, Taconi KA. The glycerin glut: options for the value-added conversion of crude glycerol resulting from biodiesel production. Environ Prog 2007;26:338–48.
[3] Delgado R, Rosas JG, Gomez N, Martinez O, Sanchez ME, Cara R. Energy valorisation of crude glycerol and corn straw by means of slow co-pyrolysis: production and characterisation of gas, char and bio-oil. Fuel 2013;112:31–7.
[4] Dou B, Song Y, Wang C, Chen H, Xu Y. Hydrogen production from catalytic steam reforming of biodiesel byproduct glycerol: issues and challenges. Renew Sustain Energy Rev 2014;30:950–60.
[5] Bartels JR, Pate MB, Olson NK. An economic survey of hydrogen production from conventional and alternative energy sources. Int J Hydrogen Energy 2010;35:8371–84.
[6] Adhikari S, Fernando SD, Haryanto A. Hydrogen production from glycerol: an update. Energy Convers Manage 2009;50:2600–4.
[7] Vaidya PD, Rodrigues AE. Glycerol reforming for hydrogen production: a review. Chem Eng Technol 2009;32:1463–9.
[8] Sad ME, Duarte HA, Vignatti Ch, Padró CL, Apesteguía CR. Steam reforming of glycerol: hydrogen production optimization. Int J Hydrogen Energy 2015;40:6097–106.
[9] Simonetti DA, Rass-Hansen J, Kunkes EL, Soares RR, Dumesic JA. Coupling of glycerol processing with Fischer-Tropsch synthesis for production of liquid fuels. Green Chem 2007;9(10):1073–83.
[10] Ramesh S, Yang EH, Jung JS, Moon DJ. Copper decorated perovskite an efficient catalyst for low temperature hydrogen production by steam reforming of glycerol. Int J Hydrogen Energy 2015;40:11428–35.
[11] Slinn M, Kendall K, Mallon C, Andrews J. Steam reforming of biodiesel byproduct to make renewable hydrogen. Bioresour Technol 2008;99:5851–8.
[12] Fermoso J, He L, Chen D. Production of high purity hydrogen by sorption enhanced steam reforming of crude glycerol. Int J Hydrogen Energy 2012;37:14047–54.
[13] Dou B, Rickett GL, Dupont V, Williams PT, Chen H, Ding Y, et al. Steam reforming of crude glycerol with in situ CO_2 sorption. Bioresour Technol 2010;101:2436–42.
[14] Veiga S, Bussi J. Steam reforming of crude glycerol over nickel supported on activated carbon. Energy Convers Manage 2017;141:79–84.
[15] Adhikari S, Fernando SD, Haryanto A. Production of hydrogen by steam reforming of glycerin over alumina-supported metal catalysts. Catal Today 2007;129:355–64.
[16] Iriondo A, Barrio VL, Cambra JF, Arias PL, Guemez MB, Navarro RM, et al. Hydrogen production from glycerol over nickel catalysts supported on Al_2O_3 modified by Mg, Zr, Ce or La. Top Catal 2008;49:46–58.
[17] Charisiou ND, Papageridis KN, Siakavelas G, Tzounis L, Kousi K, Baker MA, et al. Glycerol steam reforming for hydrogen production over Nickel supported on Alumina, Zirconia and Silica catalysts. Top Catal 2017;60(15–16):1226–50.
[18] Nichele V, Signoretto M, Menegazzo F, Gallo A, Del Santo V, Cruciani G, et al. Glycerol steam reforming for hydrogen production: design of Ni supported catalysts. Appl Catal B 2012;111–112:225–32.
[19] Wu H, La Parola V, Pantaleo G, Puleo F, Venezia AM, Liotta LF. Ni-based catalysts for low temperature methane steam reforming: recent results on Ni-Au and comparison with other bi-metallic systems. Catalysts 2013;3:563–83.
[20] Christensen KO, Chen D, Lødeng R, Holmen A. Effect of supports and Ni crystal size on carbon formation and sintering during steam methane reforming. Appl Catal A Gen 2006;314:9–22.
[21] Argyle MD, Bartholomew CH. Heterogeneous catalyst deactivation and regeneration: a review. Catalysts 2015;5:145–269.
[22] Pereñíguez R, González-De la Cruz VM, Holgado JP, Caballero A. Synthesis and characterization of a $LaNiO_3$ perovskite as precursor for methane reforming reactions catalysts. Appl Catal B Environ 2010;93:346–53.
[23] Franchini CA, Aranzaez W, Duarte de Farias AM, Pecchi G, Fraga MA. Ce-substituted LaNiO3 mixed oxides as catalyst precursors for glycerol steam reforming. Appl Catal B Environ 2014;147:193–202.
[24] Kumar N, Wang Z, Kanitkar S, Spivey JJ. Methane reforming over Ni-based pyrochlore catalyst: deactivation studies for different reactions. Appl Petrochem Res 2016;6:201–7.
[25] Vizcaíno AJ, Lindo M, Carrero A, Calles JA. Hydrogen production by steam reforming of ethanol using Ni catalysts based on ternary mixed oxides prepared by coprecipitation. Int J Hydrogen Energy 2012;3:1985–92.
[26] Bussi J, Bespalko N, Veiga S, Amaya A, Faccio R, Abello MC. The preparation and properties of Ni-La-Zr catalysts for the steam reforming of ethanol. Catal Commun 2008;10(1):33–8.
[27] Bussi J, Musso M, Veiga S, Bespalko N, Faccio R, Roger AC. Ethanol steam reforming over NiLaZr and NiCuLaZr mixed metal oxide catalysts. Catal Today 2013;213:42–9.
[28] Veiga S, Bussi J. Efficient conversion of glycerol to a H_2 rich gas mixture by steam reforming over NiLaZr catalysts. Top Catal 2016;59(2–4):186–95.
[29] Tuza PV, Souza M. Steam reforming of methane over catalyst derived from ordered double perovskite: effect of crystalline phase transformation. Catal Lett 2016;146:47–53.
[30] Pendyala DDR, Puviyarasan KVM. Analysis of effect of thermal barrier coating materials on efficiency of IC engines using 3D finite element method. IOSR J Mech Civ Eng 2014;11:53–8.
[31] Dou B, Dupont V, Williams PT, Chen H, Ding Y. Thermogravimetric kinetics of crude glycerol. Bioresour Technol 2009;100(9):2613–20.
[32] Verdonk AH. Synthesis and thermal decomposition of potassium trioxalatoaluminate hydrate. Thermochim Acta 1972;4:25–39.

Please cite this article in press as: Veiga S, et al., Hydrogen production by crude glycerol steam reforming over Ni–La–Ti mixed oxide catalysts, International Journal of Hydrogen Energy (2017), https://doi.org/10.1016/j.ijhydene.2017.10.118

[33] Scherrer P. Nachrichten von der Gesellschaft der Wissenschaften zu Göttingen. Math Phys Kl 1918;2:98–100.
[34] Bradha M, Hussain S, Chakravarty S, Amarendra G, Ashok A. Synthesis, structure and total conductivity of A-site doped $LaTiO_{3-d}$ perovskites. J Alloys Compd 2015;626:245–51.
[35] Bussi J, Musso M, Quevedo A, Faccio R, Romero M. Structural and catalytic stability assessment of Ni-La-Sn ternary mixed oxides for hydrogen production by steam reforming of ethanol. Catal Today 2017;296:154–62.
[36] Buffoni I, Pompeo F, Santori G, Nichio N. Nickel catalysts applied in steam reforming of glycerol for hydrogen production. Catal Commun 2009;10(13):1656–60.
[37] Marquevich M, Medina F, Montané D. Hydrogen production via steam reforming of sunflower oil over Ni/Al catalysts from hydrotalcite materials. Catal Commun 2001;2:119–24.
[38] Carrero A, Vizcaíno A, Calles J, García-Moreno L. Hydrogen production through glycerol steam reforming using Co catalysts supported on SBA-15 doped with Zr, Ce and La. J Energy Chem 2017;26:42–8.
[39] Charisiou ND, Siakavelas G, Papageridis KN, Baklavaridis A, Tzounis L, Polychronopoulou K, et al. Hydrogen production via the glycerol steam reforming reaction over nickel supported on alumina and lanthana-alumina catalysts. Int J Hydrogen Energy 2017;42:13039–60.
[40] Siew KW, Lee HC, Gimbun J, Chin SY, Khan MR, Taufiq-Yap YH, et al. Syngas production from glycerol-dry (CO_2) reforming over La-promoted Ni/Al_2O_3catalyst. Renew Energy 2015;74:441–7.
[41] Thyssen V, Maia T, Assaf E. Ni supported on La_2O_3–SiO_2 used to catalyze glycerol steam reforming. Fuel 2013;105:358–63.
[42] Nichele V, Signoretto M, Menegazzo F, Rossetti I, Cruciani G. Hydrogen production by ethanol steam reforming: effect of the synthesis parameters on the activity of Ni/TiO_2 catalysts. Int J Hydrogen Energy 2014;39:4252–8.
[43] Peña MA, Fierro JL. Chemical structures and performance of perovskite oxides. Chem Rev 2001;101:1981–2018.
[44] Pompeo F, Santori G, Nichio NN. Hydrogen and/or syngas from steam reforming of glycerol. Study of platinum catalysts. Int J Hydrogen Energy 2010;35:8912–20.
[45] Remón J, Giménez JR, Valiente A, García L, Arauzo J. Production of gaseous and liquid chemicals by aqueous phase reforming of crude glycerol: influence of operating conditions on the process. Energy Convers Manage 2016;110:90–112.
[46] Bobadilla LF, Penkova A, Romero-Sarria F, Centeno MA, Odriozola JA. Influence of the acid-base properties over NiSn/$MgOeAl_2O_3$ catalysts in the hydrogen production from glycerol steam reforming. Int J Hydrogen Energy 2014;39:5704–12.
[47] Araque M, Martínez TLM, Vargas JC, Centeno MA, Roger AC. Effect of the active metals on the selective H_2 production in glycerol steam reforming. App Catal B Environ 2012;125:556–66.
[48] Chiodo V, Freni S, Galvagno A, Mondello N, Frusteri F. Review. Catalytic features of Rh and Ni supported catalysts in the steam reforming of glycerol to produce hydrogen. Appl Catal A 2010;381:1–7.
[49] Valliyappan T, Bakhshi NN, Dalai AK. Pyrolysis of glycerol for the production of hydrogen or syn gas. Bioresour Technol 2008;99:4476–83.
[50] Douette AMD, Turn SQ, Wang W, Keffer VI. Experimental investigation of hydrogen production from glycerin reforming. Energy Fuels 2007;21(6):3499–504.
[51] Rajan AS, Sampath S, Shukla AK. An in situ carbon-grafted alkaline iron electrode for iron-based accumulators. Energy Environ Sci 2014;7:1110–6.
[52] Scharfenberger, Eysel. Powder diffraction file PDF 37-0804. Germany: Mineralogisch-Petrogr. Institut, Universitat Heidelberg; 1985. ICDD Grant-in-Aid.
[53] Lin KH, Wang CB, Chien SH. Catalytic performance of steam reforming of ethanol at low temperature over $LaNiO_3$ perovskite. Int J Hydrogen Energy 2013;38:3226–32.
[54] de Castro TP, Peguin RPS, Neto RCR, Borges LEP, Noronha FB. Steam reforming of Toluene over Pt/$Ce_xZr_{1-x}O_2$/Al_2O_3 catalysts. Top Catal 2016;59:292–302.
[55] Skoulou VK, Manara P, Zabaniotou AA. H_2 enriched fuels from co-pyrolysis of crude glycerol with biomass. J Anal Appl Pyrolysis 2013;99:110–6.
[56] Remón J, Mercado V, García L, Arauzo J. Effect of acetic acid, methanol and potassium hydroxide on the catalytic steam reforming of glycerol: thermodynamic and experimental study. Fuel Process Technol 2015;138:325–36.

Please cite this article in press as: Veiga S, et al., Hydrogen production by crude glycerol steam reforming over Ni–La–Ti mixed oxide catalysts, International Journal of Hydrogen Energy (2017), https://doi.org/10.1016/j.ijhydene.2017.10.118